Journal of Hazardous Materials 195 (2011) 139–146

Contents lists available at ScienceDirect

Journal of Hazardous Materials

journal homepage: www.elsevier.com/locate/jhazmat

Waste oil shale ash as a novel source of calcium for precipitated calcium carbonate: Carbonation mechanism, modeling, and product characterization

O. Velts[a,b,*], M. Uibu[a], J. Kallas[a], R. Kuusik[a]

[a] Laboratory of Inorganic Materials, Tallinn University of Technology, Ehitajate tee 5, Tallinn 19086, Estonia
[b] Laboratory of Separation Technology, Lappeenranta University of Technology, P.O. Box 20, Lappeenranta FI-53851, Finland

ARTICLE INFO

Article history:
Received 14 May 2011
Received in revised form 11 July 2011
Accepted 6 August 2011
Available online 12 August 2011

Keywords:
Oil shale ash
Precipitated calcium carbonate
Modeling
Carbonation mechanism
$CaCO_3$ polymorphs

ABSTRACT

In this paper, a method for converting lime-containing oil shale waste ash into precipitated calcium carbonate (PCC), a valuable commodity is elucidated. The mechanism of ash leachates carbonation was experimentally investigated in a stirred semi-batch barboter-type reactor by varying the CO_2 partial pressure, gas flow rate, and agitation intensity. A consistent set of model equations and physical–chemical parameters is proposed to describe the $CaCO_3$ precipitation process from oil shale ash leachates of complex composition. The model enables the simulation of reactive species (Ca^{2+}, $CaCO_3$, SO_4^{2-}, $CaSO_4$, OH^-, CO_2, HCO_3^-, H^+, CO_3^{2-}) concentration profiles in the liquid, gas, and solid phases as well as prediction of the PCC formation rate. The presence of $CaSO_4$ in the product may also be evaluated and used to assess the purity of the PCC product.

A detailed characterization of the PCC precipitates crystallized from oil shale ash leachates is also provided. High brightness PCC (containing up to ~96% $CaCO_3$) with mean particle sizes ranging from 4 to 10 μm and controllable morphology (such as rhombohedral calcite or coexisting calcite and spherical vaterite phases) was obtained under the conditions studied.

1. Introduction

In order to sustainably meet the ever-rising demand for energy, it is becoming necessary to exploit lower-quality fossil fuels such as oil shale. Well-explored oil shale reserves include the Green River deposits in the western United States, the Tertiary deposits in Queensland, Australia, the El-Lajjun deposit in Jordan, and deposits in Sweden, Estonia, France, Germany, Brazil, China, and Russia. In Estonia, large-scale combustion of calcareous kerogenous oil shale (8–12 MJ kg^{-1}) provides over 90% of the basic electric power supply. The technology used in oil shale processing for heat and power production exerts strong environmental effects. Due to the extensive use of oil shale, per capita CO_2 emissions in Estonia (15.2 metric tonnes in 2007) are about twice the European average and rank 13th worldwide [1]. In addition the process produces approximately 5–7 Mt of hazardous ash annually. A small portion of the waste ash is used for construction materials, road construction, and agricultural purposes [2], while most of the ash is transported as a slurry to be deposited on waste piles near the power plants. These ash dumps occupy an area of approximately 20 km^2. The combustion waste ash is rich in free lime and anhydrite that under aqueous conditions produces highly alkaline leachates (pH 12–13). These pose a potential long-term environmental risk as neutralization of ash fields under natural conditions may take hundreds of years [3,4].

In the context of reducing the environmental burden and enhancing economic benefit, strategies for upgrading waste ashes into products of commercial value have arisen into focus, for instance [5–8]. Related to the aforementioned issues in Estonia, the authors recently introduced a novel approach for synthesizing precipitated calcium carbonate (PCC) crystals utilizing alkaline waste ash as an alternative low-cost source of water-soluble calcium [9]. PCC is currently produced from lime in a multi-stage process that requires large amounts of energy and uses expensive high-quality raw material. PCC production using oil shale ash could have considerable commercial importance in the paint, plastics, rubber, and paper industries. Other potential advantages of this process such as safer disposal of wastes, CO_2 emissions reduction, and wastewater neutralization were elaborated in our earlier studies [10,11]. Also, a new method for intensive heterogeneous gas–liquid processing was proposed [12]. One of the main challenges in this work was establishing a quantitative understanding of heterogeneous gas–liquid–solid system kinetics and dynamics. In this paper, the mechanism of calcium carbonate precipitation during gas–liquid reaction of oil shale ash leachates is discussed as well as a mathematical model describing the precipitation process reported. The

* Corresponding author at: Laboratory of Inorganic Materials, Tallinn University of Technology, Ehitajate tee 5, Tallinn 19086, Estonia. Tel.: +372 5283756; fax: +372 620 2801.
E-mail address: olga.velts@ttu.ee (O. Velts).

0304-3894/$ – see front matter © 2011 Elsevier B.V. All rights reserved.
doi:10.1016/j.jhazmat.2011.08.019

current study also examines the impact of the complex composition of ash leachates on the main characteristics (composition, morphology, surface area, and particle size) of the solid product over a wide range of operating conditions.

2. Experimental

2.1. Preparation of alkaline mother solutions (leachates)

The leaching of Ca^{2+} and other ions from oil shale ash was previously studied by the authors [3,13,14]. In this paper, oil shale (pulverized firing) combustion ash (containing ~8.0% free CaO) was dispersed in distilled water (10:1 w/w liquid to solid ratio) under atmospheric pressure and room temperature for 15 min in a 15 L reactor equipped with a turbine-type impeller (Fig. 1(a)). The alkaline suspension was filtered from the solid ash residue. The solutions were analyzed for Ca^{2+} (titrimetric method ISO 6058:1984), SO_4^{2-}, Cl^-, K^+, PO_4^{3-} (using a Lovibond SpectroDirect spectrophotometer), CO_3^{2-}, HCO_3^-, and OH^- (titrimetric method ISO 9963–1:1994(E)). The oil shale ash leachates (pH ~12.65) had the following average ion concentration: (in g L^{-1}) Ca^{2+}: ~1.23, SO_4^{2-}: ~0.75, K^+: ~0.076, Cl^-: ~0.038, PO_4^{3-}: ~0.011 and (in mol L^{-1}) OH^-: ~0.047.

2.2. Synthesis of PCC particles

Carbonation of oil shale ash leachates was performed in a semi-batch barboter-type reactor. A turbine-type impeller was used to provide effective mechanical mixing of the gas and liquid phases to increase the interfacial contact area (Fig. 1(b)). Recirculating alkaline mother solution (*à* 10 L) was treated with a model gas mixture containing pre-determined concentrations of CO_2 in air (c_{CO_2}). The CO_2 content was based on typical industrial flue gas compositions. The flow rate (Q_G) and composition of the inlet gas were controlled using calibrated rotameters and an infrared CO_2 analyzer (Duotec). The reactor was operated batch-wise with respect to the liquid phase and continuously with respect to the gas phase. A 2^3 full-factorial experimental plan was designed in which the process variables were maintained near the center of the operating range (Table 1). Operating variables potentially influencing the precipitation conditions were varied (base value and step in parenthesis):

(a) Air–CO_2 gas mixture flow rate, Q_G (b.v. = 1000 L h^{-1}, step 500)
(b) CO_2 concentration in the inlet gas, c_{CO2} (b.v. at 25 °C and 1 atm = 5 vol%, step 5)
(c) Stirring rate, N (b.v. = 400 rpm, step 300)

Samples of the suspension were collected through a valve on the reactor body. During the carbonation experiments, the concentrations of Ca^{2+}, SO_4^{2-}, Cl^-, K^+, PO_4^{3-}, CO_3^{2-}, HCO_3^-, OH^- in the (filtered) liquid phase samples, pH (Mettler Toledo GWB SG2) and conductivity (HI9032) in the reactor, and the CO_2 content of the outlet gas flow were continuously monitored. When the pH of the solution had stabilized and the CO_2 concentration in the outlet gas became equal to the inlet values, CO_2 addition was stopped. Immediately after carbonation, the suspension was filtered (Whatman "blue ribbon" filter paper) and the resulting solid was dehydrated at 105 °C. The solid material was analyzed as received with no subsequent washing. The synthesis of PCC particles (including the preparation of alkaline mother solution from waste ash) is schematically represented in Fig. 1.

2.3. Characterization of solid products

The solid product was analyzed to determine total carbon (TC; ELTRA CS-580 Carbon/Sulfur Determinator). Phase/composition identification was carried out using X-ray diffraction (XRD), FT-IR spectroscopy and thermal analysis techniques. XRD was performed using a Bruker D8 Advanced instrument. Fourier transform infrared (FT-IR) spectra (Interspec 2020) were acquired using samples prepared as KBr pellets and using a thermoanalyzer (Setaram Setsys 1750) coupled to a FT-IR spectrometer (Nicolet 380). Determination of total sulfur and its bonding forms was carried out according to EVS 664:1995. The crystal morphology of the precipitate particles was monitored during the course of the experiment using a scanning electron microscope (Jeol JSM-8404A). The particle size distribution (PSD) of the final product was determined using a laser diffraction analyzer (Beckman Coulter LS 13320). BET-surface area and total and micropore volume were measured using a nitrogen dynamic desorption analysis method (Sorptometer KELVIN 1042). The brightness of the PCC samples was measured according to ISO 2470:1999.

3. Results and discussion

3.1. Reaction mechanism of oil shale ash leachates carbonation process

Formation of PCC from lime-containing oil shale ash is an innovative yet complex multi-stage process. Recently, the mechanisms and modeling algorithms for intermediate stages of the process including calcium leaching [3,13], dissolution of gaseous CO_2 into the alkaline liquid phase [15], and calcium carbonate precipitation via CO_2 absorption into pure lime based model solutions [16] have been reported by the authors.

In the present study, a mechanism for the reaction of CO_2 with Ca^{2+} and SO_4^{2-} rich alkaline oil shale ash leachates is proposed. The carbonation process is described by Eqs. (1)–(9) beginning with the physical dissolution of gaseous CO_2 into solution:

$$CO_2(q) \leftrightarrow CO_2(l) \quad (1)$$

The solubility equilibrium follows Henry's law (at pressures below approximately 5 atm):

$$[CO_2(l)]_{eq} = k_H \times P_{CO_2} \quad (2)$$

where k_H is the Henry's law constant and P_{CO_2} is the CO_2 partial pressure.

Formation of bicarbonate:

$$CO_2(l) + OH^- \underset{k_{12}}{\overset{k_{11}}{\rightleftarrows}} HCO_3^- \quad (3)$$

Dissociation of bicarbonate:

$$HCO_3^- + OH^- \underset{k_{22}}{\overset{k_{21}}{\rightleftarrows}} CO_3^{2-} + H_2O \quad (4)$$

Ionization of water:

$$OH^- + H^+ \underset{k_{32}}{\overset{k_{31}}{\rightleftarrows}} H_2O \quad (5)$$

CO_2 hydration [17]:

$$CO_2(l) + H_2O \underset{k_{42}}{\overset{k_{41}}{\rightleftarrows}} HCO_3^- + H^+ \quad (6)$$

Nucleation and growth of $CaCO_3$ crystals:

$$Ca^{2+} + CO_3^{2-} \underset{k_{52}}{\overset{k_{51}}{\rightleftarrows}} CaCO_3 \quad (7)$$

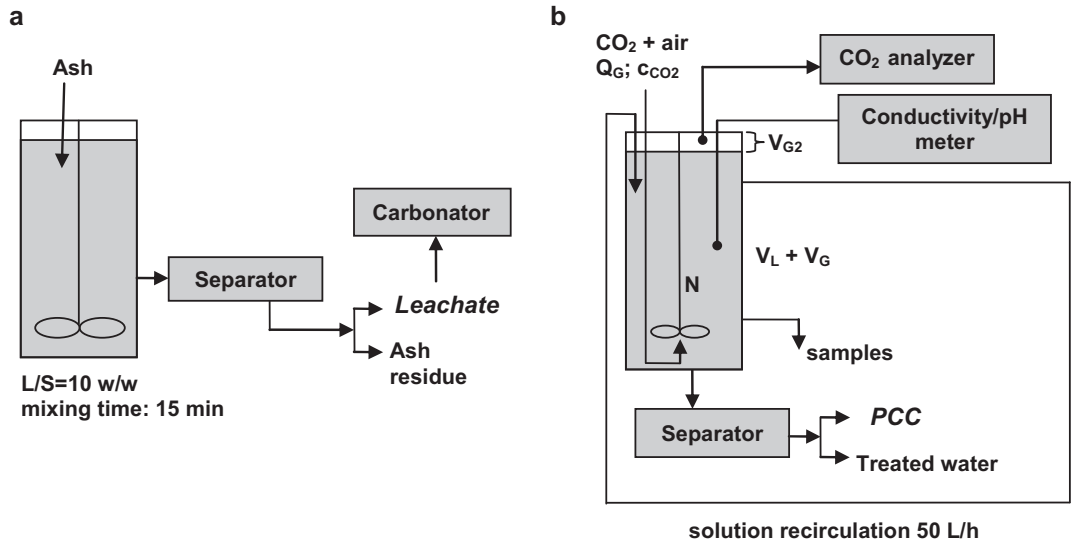

Fig. 1. Principal experimental scheme: (a) leaching step; (b) carbonation step.

Formation of anhydrate phase:

$$Ca^{2+} + SO_4{}^{2-} \leftrightarrow CaSO_4 \quad (8)$$

Back-dissolution of $CaCO_3$ crystals at lower pH:

$$CaCO_3 + H^+ \underset{k_{62}}{\overset{k_{61}}{\rightleftarrows}} Ca^{2+} + HCO_3^- \quad (9)$$

The reactions of other ions present such as K^+, Cl^-, and $PO_4{}^{3-}$ were neglected as their concentrations in the solution remained unchanged during carbonation. It is therefore assumed that they do not take part in the precipitation process in significant amounts.

3.2. Modeling of calcium carbonate precipitation from oil shale ash leachates

The model proposed in this paper accounts for absorption and reaction kinetics taking place in the liquid phase (Eqs. (1)–(9)), including formation of the solid product, as well as the hydrodynamic conditions within the system. The concentration profiles of all species participating in the precipitation process may be modeled as a function of time using the following differential equations (assuming that the system is operated isothermally at 25 °C):

- For CO_2 dissolved in the liquid phase:

$$\frac{d[CO_2(l)]}{dt} = \frac{k_L a^0_{CO_2} \times E \times \sum_{i=1}^{n} \left(\left(\frac{k_H \times M_{CO_2} \times P \times [CO_2{}^i(g)]}{\rho_{CO_2}} - [CO_2(l)] \right) \times \frac{V_L + V_G}{n} \right)}{V_L} - k_{11}[CO_2(l)][OH^-] + k_{12}[HCO_3^-] - k_{41}[CO_2(l)] + k_{42}[HCO_3^-][H^+] \quad (10)$$

- For Ca^{2+}, OH^-, $SO_4{}^{2-}$, $HCO_3{}^-$, $CO_3{}^{2-}$, and H^+ ions:

$$\frac{d[Ca^{2+}]}{dt} = k_{52} - k_{51}[Ca^{2+}][CO_3{}^{2-}] + k_L a_{CaSO_4} \times ([SO_4{}^{2-}]^* - [SO_4{}^{2-}]) + k_{61}[H^+] - k_{62}[Ca^{2+}][HCO_3{}^-] \quad (11)$$

$$\frac{d[OH^-]}{dt} = -k_{11}[CO_2(l)][OH^-] + k_{12}[HCO_3{}^-] - k_{21}[HCO_3{}^-][OH^-] + k_{22}[CO_3{}^{2-}] + k_{32} - k_{31}[OH^-][H^+] \quad (12)$$

$$\frac{d[SO_4{}^{2-}]}{dt} = k_L a_{CaSO_4} \times ([SO_4{}^{2-}]^* - [SO_4{}^{2-}]) \quad (13)$$

$$\frac{d[HCO_3{}^-]}{dt} = k_{11}[CO_2(l)][OH^-] - k_{12}[HCO_3{}^-] - k_{21}[HCO_3{}^-][OH^-] + k_{22}[CO_3{}^{2-}] + k_{41}[CO_2(l)] - k_{42}[HCO_3{}^-][H^+] + k_{61}[H^+] - k_{62}[Ca^{2+}][HCO_3{}^-] \quad (14)$$

$$\frac{d[CO_3{}^{2-}]}{dt} = k_{21}[HCO_3{}^-][OH^-] - k_{22}[CO_3{}^{2-}] + k_{52} - k_{51}[Ca^{2+}][CO_3{}^{2-}] \quad (15)$$

$$\frac{d[H^+]}{dt} = k_{32} - k_{31}[OH^-][H^+] + k_{41}[CO_2(l)] - k_{42}[HCO_3{}^-][H^+] - k_{61}[H^+] + k_{62}[Ca^{2+}][HCO_3{}^-] \quad (16)$$

Table 1
Parameters of the oil shale ash leachates carbonation experiments.

Nr	Q_G (L h^{-1})	Air flow rate (L h^{-1})	CO_2 flow rate (L h^{-1})	c_{CO_2} (vol%)	N[a] (rpm)
1	1000	950	50	5	400
2	1000	950	50	5	1000
3	1000	850	150	15	400
4	1000	850	150	15	1000
5	2000	1900	100	5	400
6	2000	1900	100	5	1000
7	1500	1350	150	10	700
8	2000	1700	300	15	400
9	2000	1700	300	15	1000

[a] The stirring rate, as measured experimentally, corresponds to a power consumption 1.1, 2.0 and 3.7 W L^{-1} for N = 400, 700 and 1000 rpm, respectively.

- For CO_2 exiting the ith section of the reaction mixture:

$$\frac{d[CO_2{}^i(g)]}{dt} = \frac{Q_G([CO_2(g)]_{IN} - [CO_2{}^i(g)]) - k_L a^0_{CO_2} \times E \times ((k_H \times M_{CO_2} \times P \times [CO_2{}^i(g)]/\rho_{CO_2}) - [CO_2(l)]) \times (V_L + V_G)/n}{V_G/n} \quad (17)$$

- For CO_2 exiting the reactor e.g. headspace V_{G2} above the reaction mixture (see Fig. 1(b)):

$$\frac{d[CO_2(g)]_{OUT}}{dt} = \frac{Q_G([CO_2(g)] - [CO_2(g)]_{OUT})}{V_{G_2}} \quad (18)$$

- For $CaCO_3$ forming during the carbonation process:

$$\frac{d[CaCO_3]}{dt} = k_{51}[Ca^{2+}][CO_3{}^{2-}] - k_{52} - k_{61}[H^+] + k_{62}[Ca^{2+}][HCO_3{}^-] \quad (19)$$

- For $CaSO_4$ forming during the carbonation process:

$$\frac{d[CaSO_4]}{dt} = k_L a_{CaSO_4} \times ([SO_4{}^{2-}] - [SO_4{}^{2-}]^*) \quad (20)$$

In Eqs. (10)–(20) concentrations are expressed in molar units, Q_G is the gas volumetric flow rate in L s^{-1}, $k_L a^0_{CO_2}$ is the volumetric mass transfer coefficient of CO_2 in the absence of chemical reaction in s^{-1}, E is the CO_2 mass transfer enhancement factor, V_L is the solution volume in L, V_G is the volume of gas in the gas–liquid mixture in L, V_{G2} is the gas volume in the reactor headspace in L, k_H is the Henry's Law constant in mol·(L atm)$^{-1}$, P is the atmospheric pressure in atm, M_{CO_2} is the CO_2 molar mass in g mol^{-1}, and ρ_{CO_2} is the CO_2 gas density in g L^{-1}.

A program feature accounting for changes in V_L, V_G, and V_{G2} due to sample collection was implemented in the modeling algorithm. The gas phase in the reaction mixture was divided into a number of theoretical sections n with a volume V_G/n (gas phase in approximately plug flow, liquid phase in perfectly mixed flow due to solution recirculation). Each of these sections (high correlation coefficient observed at $n = 10$) was treated as a non-equilibrium stage governed by Eq. (17).

Considering the near infinite-dilution ionic strength of the leachates ($I = 0.1$), the value of the second-order rate constant k_{11} (in L (mol s)$^{-1}$) of reaction (3) was calculated as a function of temperature T (K) using a relationship proposed by Pohorecki and Moniuk [18]:

$$\log\ k_{11} = 11.916 - \frac{2382}{T} \quad (21)$$

The backward reaction rate k_{12} in Eq. (3) is defined by the value of the equilibrium constant for this reaction ($k_{12} = k_{11}K_w/K_1$). The value of the solubility product K_w (mol^2 m^{-6}) is given by Tsonopoulos [19]:

$$\log\left(\frac{K_w}{\rho_w^2}\right) = -\frac{5839.5}{T} - 22.4773\ \log(T) + 61.2062 \quad (22)$$

The value of the equilibrium constant K_1 (mol m^{-3}) is given as a function of temperature by Edwards et al. [20]:

$$K_1 = \exp\left(-\frac{12092.1}{T} - 36.786\ \ln(T) + 235.482\right)\rho_w \quad (23)$$

where ρ_w is the density of water (kg m^{-3}).

The reaction rate constant k_{21} of reaction (4) was reported as 6×10^6 m^3 (mol s)$^{-1}$ by Eigen [21]. The equilibrium constant K_2 (m^3 mol^{-1}) at infinite dilution that determines the value of the backward reaction rate, $k_{22} = k_{21}/K_2$, is given by Hikita et al. [22]:

$$\log(K_2) = \frac{1568.9}{T} - 2.5866 - 6.737 \times 10^{-3}T \quad (24)$$

The neutralization rate constant, k_{31}, was determined by Eigen [21] to be 1.4×10^8 m^3 (mol s)$^{-1}$. The rate constant k_{41} for the reaction between CO_2 and water is 0.024 s^{-1} [23]. The values of the backward reaction rate constants k_{32} and k_{42} may be calculated from the equilibrium constants and are equal to k_{31}/K_w and k_{41}/K_1.

The value of the Henry's law constant k_H (mol (L bar)$^{-1}$) may be expressed as a function of temperature using the equation of Pohorecki and Moniuk [24]:

$$\log\ k_H = 9.1229 - 5.9044 \times 10^{-2}T + 7.8857 \times 10^{-5}T^2 \quad (25)$$

The average values of the reaction rate constants k_{51} and k_{52} in Eq. (7) were estimated by Velts et al. [16] to be 1.88×10^6 L (mol s)$^{-1}$ and 0.009 mol (L s)$^{-1}$. Based on our study of CO_2 uptake kinetics in hydroxide solutions under various process conditions [15], the volumetric CO_2 mass transfer coefficients for the system in the absence of chemical reaction $k_L a^0_{CO_2}$ (s^{-1}) were calculated using an empirical equation ($R^2 = 0.91$) applicable to barboter-type reactors:

$$k_L a^0_{CO_2} = 2.953 \times 10^{-3} \times \left(\frac{Q_G}{V_L}\right)^{0.386}\left(\frac{P_N}{V_L}\right)^{0.330} c_{CO_2}^{0.114} \quad (26)$$

in which P_N is the power consumed by the stirrer in watts.

The effect of chemical reaction on the process performance was accounted for by introducing the CO_2 mass transfer enhancement factor, E. This value was determined using an empirical equation ($R^2 = 0.97$) proposed by Velts et al. [16], where E is a function of the initial Ca^{2+} concentration (mmol L^{-1}):

$$E = 0.0027 \times [Ca^{2+}]_0^2 + 0.0224 \times [Ca^{2+}]_0 + 1.0 \quad (27)$$

Based on the experimental data obtained in this study, the $SO_4{}^{2-}$ dynamic equilibrium concentration $[SO_4{}^{2-}]^*$ (mmol L^{-1}) was calculated using an empirical equation ($R^2 = 0.98$) dependent on the operating parameters and the initial concentrations of Ca^{2+} and $SO_4{}^{2-}$ ions (mmol L^{-1}) in the leachate:

$$[SO_4{}^{2-}]^* = 0.761 \times [SO_4{}^{2-}]_0{}^{0.976}[Ca^{2+}]_0{}^{-0.073} \times \left(\frac{Q_G}{V_L}\right)^{0.066} c_{CO_2}{}^{0.038}\left(\frac{P_N}{V_L}\right)^{-0.012} \quad (28)$$

The volumetric mass transfer coefficient of anhydrite, $k_L a_{CaSO_4}$ and the reaction rate constants k_{61} and k_{62} in Eq. (9) were evaluated from the differential equations (10)–(20). The set of model equations was solved by means of linear multi-step methods implemented in ODESSA, which is based on the LSODE software [25]. The calculations were performed using the MODEST 6.1 software package [26] designed for various model-building tasks such as simulation, parameter estimation, sensitivity analysis, and optimization. The software consists of a FORTRAN 95/90 library of objective functions, solvers, and optimizers linked to model problem-dependent routines and the objective function.

Based on the estimated values of $k_L a_{CaSO_4}$ (s^{-1}), an empirical equation ($R^2 = 0.8$) applicable to barboter-type reactors was proposed as a function of the main process parameters:

$$k_L a_{CaSO_4} = 1.95 \times 10^{-7} \times \left(\frac{Q_G}{V_L}\right)^{1.702} c_{CO_2}{}^{1.134}\left(\frac{P_N}{V_L}\right)^{0.126} \quad (29)$$

The average values of the reaction rate constants k_{61} and k_{62} were estimated to be 0.1 ($\pm$0.021)$\times 10^7$ s^{-1} and 0.4 ($\pm$0.013)$\times 10^3$ L (mol s)$^{-1}$. The correlation coefficients for all data sets were greater than 0.93. The reaction rate constants used in Eqs. (3)–(9) and other parameters used in this paper ($T = 298.1$ K) are summarized in Table 2.

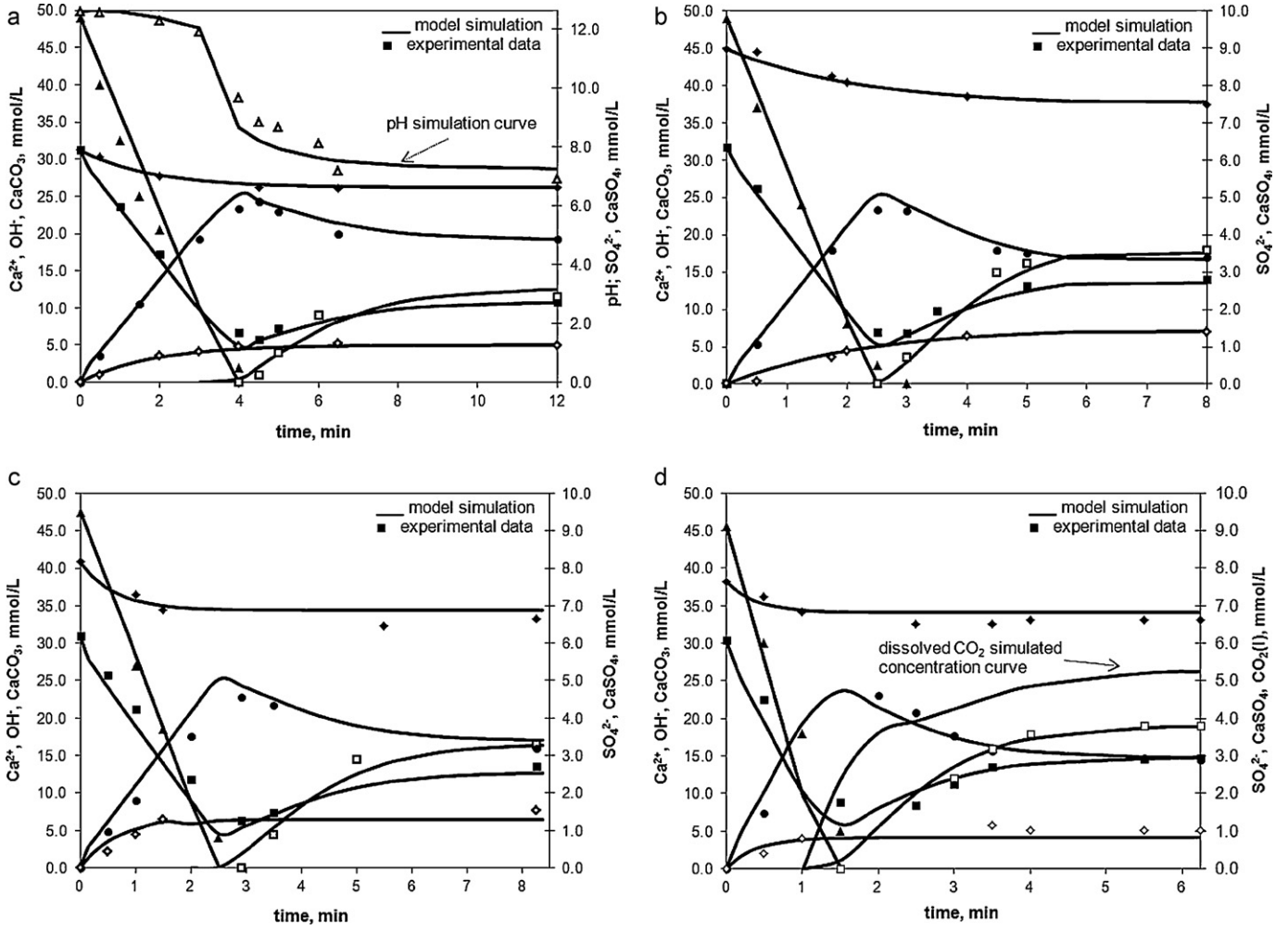

Fig. 2. Modeling of ash leachate carbonation process accompanied by the formation of PCC at (a): $Q_G = 2000\,L\,h^{-1}$, $c_{CO_2} = 5$ vol%; $N = 1000$ rpm; (b): $Q_G = 1000\,L\,h^{-1}$, $c_{CO_2} = 15$ vol%; $N = 1000$ rpm; (c): $Q_G = 1500\,L\,h^{-1}$, $c_{CO_2} = 10$ vol%; $N = 700$ rpm; (d): $Q_G = 2000\,L\,h^{-1}$, $c_{CO_2} = 15$ vol%; $N = 400$ rpm: experimental vs. simulated Ca^{2+} (■), SO_4^{2-} (♦), OH^- (▲), $CaCO_3$ (●), $CaSO_4$ (◊), HCO_3^- (□), CO_2(l) concentration (mmol L^{-1}) and pH (Δ) profiles.

The model was verified by comparing the predictions of concentration changes for the reactive species (Ca^{2+}, OH^-, SO_4^{2-}, $CaCO_3$, $CaSO_4$, HCO_3^-, CO_2, H^+, and CO_3^{2-}) with the experimental data. Plots of experimental and simulated concentration profiles corresponding to experiments 4, 6, 7, and 8 (Table 1) are provided in Fig. 2. The relatively small deviations between the measured and estimated data confirm the ability of the proposed model to quite accurately describe the process course including re-dissolution of PCC due to increased solubility of $CaCO_3$ at lower pH. It is also worth emphasizing that the model enables the prediction of pH (Fig. 2(a)), which suggests potential applications in wastewater neutralization process design.

Table 2
Parameters used in the modeling of oil shale ash leachates carbonation at 298 K.

Parameter	Value	Parameter	Value
k_{11} (L(mol s)$^{-1}$)	8.4×10^3	k_{42} (L(mol s)$^{-1}$)	5.7×10^4
k_{12} (s^{-1})	2.0×10^{-4}	k_{51}^{av} (L(mol s)$^{-1}$)	1.9×10^6
k_{21} (L(mol s)$^{-1}$)	6.0×10^9	k_{52}^{av} (mol(L s)$^{-1}$)	9.0×10^{-3}
k_{22} (s^{-1})	1.2×10^6	k_{61}^{av} (s^{-1})	0.1×10^7
k_{31} (L(mol s)$^{-1}$)	1.4×10^{11}	k_{62}^{av} (L(mol s)$^{-1}$)	0.4×10^3
k_{32} (mol·(L s)$^{-1}$)	1.3×10^{-3}	k_H (mol(L atm)$^{-1}$)	3.5×10^{-2}
k_{41} (s^{-1})	2.4×10^{-2}	ρ_{CO_2} (25 °C) (kg m^{-3})	1.8×10^0

3.3. Characterization of PCC crystallized from oil shale ash leachates

Among other parameters, the shape, size, and texture of crystals play a crucial role in determining the properties and application suitability of a material. For this reason, a detailed characterization of the final precipitates formed during ash leachate carbonation under different conditions was performed. The characteristics of samples PCC1–PCC9 were determined using numerous characterization techniques (see Section 2.3) and are presented in Table 3. The unwashed precipitates were a bright white color with a fine and powdery texture. The brightness value (~93%) exceeded that of PCC (~89%) obtained from pure lime under the same conditions [9]. Total carbon (TC) analysis indicated that the solid samples predominantly contained $CaCO_3$ (~94.3–96.2%), with minor amounts of $CaSO_4$ (~4–6%), evidently adsorbed on the surface of the $CaCO_3$ crystals (Table 3). Washing of the precipitate cake would be expected to improve the purity of the solid product by a few percentage points. The phase composition was also confirmed using FT-IR spectroscopy.

The morphology of the precipitated particles was examined using scanning electron microscopy (SEM). Fig. 3 contains SEM images of the final precipitates PCC1–PCC9 crystallized under various carbonation conditions (Table 3). Under the conditions in experiments 1–5 (Table 1), well-defined rhombohedral

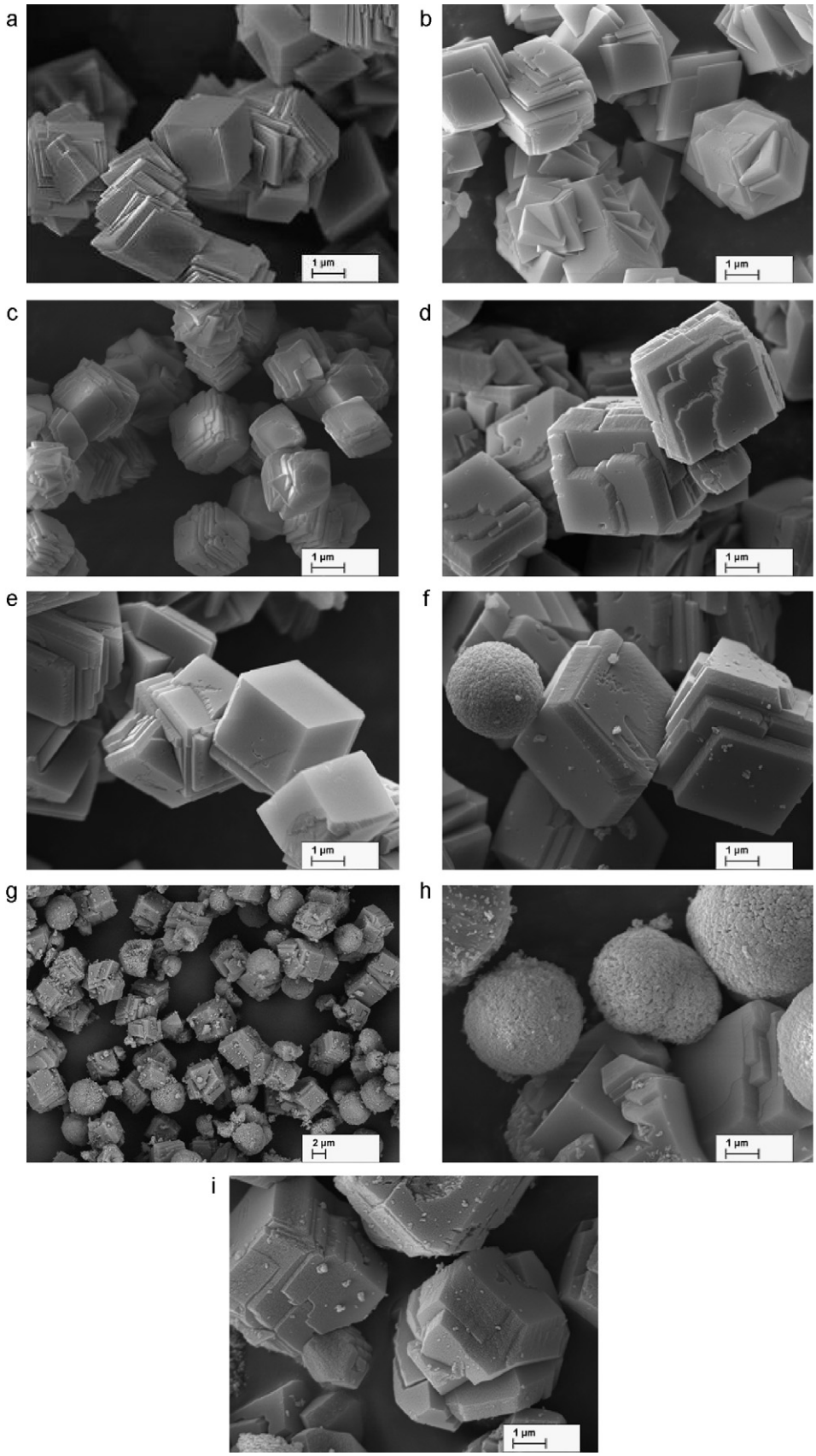

Fig. 3. SEM micrographs of PCC samples (a) PCC1, (b) PCC2, (c) PCC3, (d) PCC4, (e) PCC5, (f) PCC6, (g) PCC7, (h) PCC8, (i) PCC9 formed via oil shale ash leachate carbonation under experimental conditions presented in Table 1.

Table 3
Synthesis conditions and main characteristics of oil shale ash leachates carbonation products.

Sample	Operating variables			Solid product characteristics								
	Q_G (L h^{-1})	c_{CO_2} (vol%)	N (rpm)	$CaCO_3^{av}$ (%)			$CaSO_4^{av}$ (%)	SSA (m^2 g^{-1})	V_{tot} (mm^3 g^{-1})	V_{micro} (mm^3 g^{-1})	D_{mean} (μm)	Brightness ISO (%)
				TC	XRD							
					calcite	*vaterite*						
PCC1	1000	5	400	94.5			5.7	2.28	3.38	–	4.1	93.2
PCC2	1000	5	1000	94.5			5.8	2.56	3.51	0.11	5.1	
PCC3	1000	15	400	94.6	100.0		5.5	3.15	4.03	–	4.8	
PCC4	1000	15	1000	94.4			5.9	1.33	1.93	–	7.8	
PCC5	2000	5	400	94.4			5.9	1.35	1.74	–	6.5	
PCC6	2000	5	1000	95.1	97.3	2.6	5.0	2.38	3.77	–	8.1	92.7
PCC7	1500	10	700	95.6	77.2	21.9	4.4	4.70	11.05	0.01	7.7	92.3
PCC8	2000	15	400	96.2	63.2	36.3	4.0	7.29	17.44	0.43	8.0	
PCC9	2000	15	1000	95.4	95.7	3.6	4.5	1.95	3.44	–	9.9	

crystals with a mean size ranging from ~4 to 8 μm were produced (Fig. 3(a–e)). X-ray powder diffraction analysis (XRD) of these carbonated samples (PCC1–PCC5) identified calcite as the only crystal form of calcium carbonate detected. Carbonation under the intensified hydrodynamic conditions (experiments 6–8, Table 1) resulted in formation of distinctly spherical particles in the precipitates along with the rhombohedral crystals of calcium carbonate (Fig. 3(f–h)). Initial analysis of these images indicated that the rhombohedral crystal was calcite, while the calcium carbonate microspheres were forms of vaterite. The coexistence of calcite and vaterite in the product (PCC6–PCC9) was confirmed using XRD measurements (Table 3), which enabled us to distinguish different morphologies of PCC. The XRD results indicated that sample PCC6 contained only small amount of the vaterite phase (2.6%), while the relative mass percentages of vaterite in samples from experiments 7 and 8 were ~22 and 36% (Table 3). The presence of a significant amount of spherical vaterite could explain the greater surface area and pore volume in samples PCC7 and PCC8. The shape and surface observations confirmed the results of the particle size distribution analysis. Interestingly, precipitation under the most rapid conditions (experiment 9, Table 1) decreased the amount of vaterite in the product, leading to formation of pseudo-cubic or randomly aggregated rhombohedral (Fig. 3(i)) and spherical structures with a mean diameter of ~10 μm and a calcite content of ~96% (PCC9, Table 3).

The results suggest that the carbonation conditions may direct the morphology of the $CaCO_3$ crystals and indicate that the coexisting vaterite polymorph can be stabilized under specific experimental conditions. Whether the vaterite phase is formed prior to or during the PCC re-dissolution stage is a matter of great interest and requires further investigation. A closer examination of the morphological development of the $CaCO_3$ crystals at different crystallization times will be undertaken.

4. Conclusion

In this study, modeling, simulation, and experimental results describing the carbonation of leachates from oil shale ash are presented. This work is part of our effort to develop a promising calcium carbonate production process employing an abundant waste material.

A mathematical model of the multi-step PCC formation process incorporating mechanisms of CO_2 dissolution and $CaCO_3$ and $CaSO_4$ precipitation was introduced. The model provided results that were in good agreement with experimental data, confirming its accuracy. The modeling algorithm presented in this paper may be applied to design, energetic, and economic assessment of PCC pilot plants using oil shale ash or other lime-containing wastes or calcium-rich wastewaters as feedstock.

Carbonation of oil shale ash leachates resulted in precipitation of high brightness PCC containing up to ~96% $CaCO_3$ with mean particle sizes ranging from 4 to 10 μm. Depending on the carbonation conditions, formation of rhombohedral calcite crystals or co-precipitation of calcite and spherical vaterite structures occurred, suggesting control over $CaCO_3$ crystallization and the ability to construct crystals with a desired morphology. The PCC morphogenesis will be further investigated to determine the relationship between formation conditions and morphology.

A description of the carbonation reaction mechanism and the properties of the precipitated product are important for understanding and estimating the potential reusability of alkaline wastes associated with oil shale-based power production. According to simplified calculations, 1 tonne of ash (containing ~20% of free lime on the average) would allow producing near to 360 kg of $CaCO_3$, while via carbonation of 1 m^3 of leachates at least 1.3 kg of CO_2 can be captured and up to 3 kg of PCC formed. Due to availability of enormously large amounts (10–15 million m^3) of highly alkaline ash leachates in the proximity of CO_2 emission source, the direct capture and storage of CO_2-containing flue gas by leachates could further improve the technology. Hence, oil shale energetics could benefit from this innovative process by utilizing and valorizing its own waste-products into a valuable commodity, lowering the environmental impact of deposited waste material, alkaline leachates and CO_2 emissions at the same time.

Acknowledgements

The financial support of the Estonian Ministry of Education and Research (SF0140082s08) and the Estonian Science Foundation (Grant No. 7379) are gratefully acknowledged. The assistance of Prof. Kalle Kirsimäe and Dr. Valdek Mikli in performance of XRD and SEM measurements is highly appreciated. Authors are also grateful for the contribution of Esko Kukkamäki (UPM-Kymmene Corporation). This work has been partially supported by graduate school "Functional materials and processes" receiving funding from the European Social Fund under project 1.2.0401.09-0079 in Estonia.

References

[1] Carbon Dioxide Information Analysis Center, Environmental Sciences Division (US), CO_2 emissions—Estonia. Available at: http://data.worldbank.org/indicator/EN.ATM.CO2E.PC/countries/EE-7E-XR (accessed May 2011).
[2] A. Ots, Oil Shale Fuel Combustion, Tallinn University of Technology Press, Tallinn, 2006.
[3] O. Velts, M. Hautaniemi, J. Kallas, M. Kuosa, R. Kuusik, Modeling calcium dissolution from oil shale ash: part 2. Continuous washing of the ash layer, Fuel Process. Technol. 91 (5) (2010) 491–495.
[4] R. Mõtlep, T. Sild, E. Puura, K. Kirsimäe, Composition, diagenetic transformation and alkalinity potential of oil shale ash sediments, J. Hazard. Mater. 184 (1–3) (2010) 567–573.

[5] A.S.M. Ribeiro, R.C.C. Monteiro, E.J.R. Davim, M.H.V. Fernandes, Ash from a pulp mill boiler—characterisation and vitrification, J. Hazard. Mater. 179 (1–3) (2010) 303–308.
[6] C. Ferreira, A. Ribeiro, L. Ottosen, Possible applications for municipal solid waste fly ash, J. Hazard. Mater. 96 (2–3) (2003) 201–216.
[7] R. Cioffi, M. Marroccoli, L. Sansone, L. Santoro, Potential application of coal–fuel oil ash for the manufacture of building materials, J. Hazard. Mater. 124 (1–3) (2005) 101–106.
[8] Yu-Fen Yang, Guo-Sheng Gai, Zhen-Fang Cai, Qing-Ru Chen, Surface modification of purified fly ash and application in polymer, J. Hazard. Mater. 133 (1–3) (2006) 276–282.
[9] O. Velts, M. Uibu, J. Kallas, R. Kuusik, Prospects in waste oil shale ash sustainable valorization, World Acad. Sci. Eng. Technol. 76 (2011) 451–455.
[10] M. Uibu, M. Uus, R. Kuusik, CO_2 mineral sequestration in oil-shale wastes from Estonian power production, J. Environ. Manage. 90 (2) (2009) 1253–1260.
[11] M. Uibu, O. Velts, R. Kuusik, Developments in CO_2 mineral carbonation of oil shale ash, J. Hazard. Mater. 174 (1–3) (2010) 209–214.
[12] R. Kuusik, M. Uus, M. Uibu, et al., Method for neutralization of alkaline waste water with carbon dioxide included in flue gas, Patent nr EE05349B1.
[13] O. Velts, M. Hautaniemi, J. Kallas, R. Kuusik, Modeling calcium dissolution from oil shale ash: part 1. Ca dissolution during ash washing in a batch reactor, Fuel Process. Technol. 91 (5) (2010) 486–490.
[14] O. Velts, M. Uibu, I. Rudjak, J. Kallas, R. Kuusik, Utilization of oil shale ash to prepare PCC: leachibility dynamics and equilibrium in the ash–water system, Energy Procedia 1 (1) (2009) 4843–4850.
[15] O. Velts, M. Hautaniemi, M. Uibu, J. Kallas, R. Kuusik, Modelling of CO_2 mass transfer and hydrodynamics in a semi-batch reactor, J. Int. Sci. Publ. Mater. Methods Technol. 4 (2) (2010) 68–79. Available at: http://www.science-journals.eu/mmt/index.html (accessed May 2011).
[16] O. Velts, M. Uibu, J. Kallas, R. Kuusik, CO_2 mineral trapping: modeling of calcium carbonate precipitation in a semi-batch reactor, Energy Procedia 4 (2011) 771–778.
[17] A.H.G. Cents, D.W.F. Brilman, G.F. Versteeg, CO_2 absorption in carbonate/bicarbonate solutions: the Danckwerts-criterion revisited, Chem. Eng. Sci. 60 (2005) 5830–5835.
[18] R. Pohorecki, W. Moniuk, Calculation of the rate constant for the reaction of carbon dioxide with hydroxyl ions in mixed electrolyte solutions, Rep. Inst. Chem. Eng. Warsaw. Tech. Univ. 5 (1976) 179–192.
[19] C. Tsonopoulos, Ionization constants of water pollutants, J. Chem. Eng. Data 21 (1976) 190–193.
[20] T.J. Edwards, G. Maurer, J. Newman, J.M. Prausnitz, Vapor–liquid equilibria in multicomponent aqueous solution of volatile weak electrolytes, AIChE J. 24 (1978) 966–976.
[21] M. Eigen, Protonenübertagung, säure-base-katalyse und enzymatische hydrolyse. teil I: Elementarvorgänge, Angew. Chem. 75 (1963) 489–508.
[22] H. Hikita, S. Asai, T. Takatsuka, Absorption of carbon dioxide into aqueous sodium hydroxide and sodium bicarbonate solutions, Chem. Eng. J. 11 (1976) 131–141.
[23] P.V. Danckwerts, M.M. Sharma, Absorption of carbon dioxide into solutions of alkalis and amines, Chem. Eng. (London) 10 (1966) 244–280.
[24] R. Pohorecki, W. Moniuk, Kinetics of reaction between carbon dioxide and hydroxyl ions in aqueous electrolyte solutions, Chem. Eng. Sci. 43 (1988) 1677–1684.
[25] A.C. Hindmarsh, ODEPACK, a systematized collection of ODE solvers, Sci. Comput. IMACS Trans. Sci. Comput. 1 (1983) 55–64.
[26] H. Haario, Modest user manual, Profmath Oy, Finland, 1994.